Journal Pre-proof

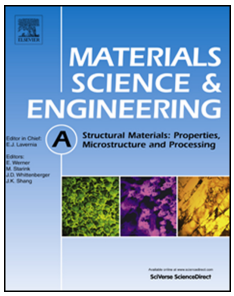

Effects of W micro-additions on precipitation kinetics and mechanical properties of an Al-Mn-Mo-Si-Zr-Sc-Er alloy

Shipeng Shu, Anthony De Luca, David C. Dunand, David N. Seidman

PII: S0921-5093(20)31613-0

DOI: https://doi.org/10.1016/j.msea.2020.140550

Reference: MSA 140550

To appear in: *Materials Science & Engineering A*

Received Date: 27 September 2020

Revised Date: 10 November 2020

Accepted Date: 14 November 2020

Please cite this article as: S. Shu, A. De Luca, D.C. Dunand, D.N. Seidman, Effects of W micro-additions on precipitation kinetics and mechanical properties of an Al-Mn-Mo-Si-Zr-Sc-Er alloy, *Materials Science & Engineering A*, https://doi.org/10.1016/j.msea.2020.140550.

CRediT authorship contribution statement

Shipeng Shu: Investigation, Formal analysis, Writing - original draft, Writing - review & editing. Anthony De Luca: Investigation, Formal analysis, Writing - review & editing. David C. Dunand: Funding acquisition, Formal analysis, Writing - review & editing, Supervision. David N. Seidman: Funding acquisition, Formal analysis, Writing - review & editing, Supervision.

Effects of W micro-additions on precipitation kinetics and mechanical properties of an Al-Mn-Mo-Si-Zr-Sc-Er alloy

Shipeng Shu[1], *Anthony De Luca*[1, 2], *David C. Dunand*[1], *David N. Seidman*[1,3]

[1] Northwestern University, Department of Materials Science and Engineering, 2220 Campus Drive, Evanston, IL 60208 USA

[2] Empa, Swiss Federal Laboratories for Materials Science and Technology, Laboratory for Advanced Materials Processing, Überlandstrasse 129, CH-8600 Dübendorf, Switzerland

[3] Northwestern University Center for Atom-Probe Tomography, 2220 Campus Drive, Evanston, IL 60208 USA

Abstract

A micro-addition (0.025 at.%) of slow-diffusing W to an Al-0.26Mn-0.11Mo-0.11Si-0.08Zr-0.02Sc-0.01Er (at.%) alloy accelerates $L1_2$-Al_3(Zr,Sc) precipitation but retards α-Al(Mn,Mo)Si precipitation. The W micro-addition increases the peak-microhardness of the alloy during isothermal aging but does not improve the coarsening resistance and creep resistance.

Keywords: aluminum alloys; precipitation kinetics; atom-probe tomography; elevated-temperature.

Aluminum alloys strengthened by $L1_2$-Al_3Sc nano-precipitates exhibit excellent creep- and coarsening resistance at elevated temperatures (up to 425 °C) compared to conventional precipitation-strengthened Al alloys (such as 2xxx series), particularly when they are further modified with rare-earth and transition metal elements [1-7]. Specifically, previous studies focused on: (i) increasing the Al-matrix(f.c.c.)/$L1_2$-precipitate lattice parameter mismatch by introducing lanthanoids, such as Er and Y [8-11]; (ii) improving $L1_2$-precipitate coarsening resistance by introducing slow-diffusing transition metals, Zr, Ti and V, which partition to the $L1_2$-precipitates [12-17]; (iii) stimulating $L1_2$ nucleation kinetics by adding elements such as Si, Ge, Sn, In and Sb [18-20]; and (iv) reducing cost by replacing Sc with other $L1_2$-forming elements, Zr and Ti [21-23]. De Luca et al. demonstrated that small additions of Er, Zr and Si to an Al-Sc alloy at a very low Sc concentration, 0.014 at.%, results in an optimized Al-0.08Zr-0.014Sc-0.008Er-0.09Si (at.%) alloy with excellent $L1_2$-precipitate coarsening resistance at 400 °C, and good creep resistance at 300 °C (threshold stress ~17 MPa), at a fraction of the cost of alloys with a higher Sc concentration and comparable coarsening/creep resistance [23]. Recently, the addition of Mn and Mo to this Sc-lean alloy was demonstrated to introduce a second population of precipitates, α-Al(Mn,Mo)Si, in addition to the $L1_2$-precipitates, leading to further improvements of the microstructural stability and mechanical properties [24, 25]. Manganese provides solid-solution strengthening and also serves as the α-Al(Mn,Mo)Si former (with Si) [6]; slow-diffusing Mo [26] is also a solid-solution strengthener and partitions to $L1_2$- and α-precipitates, significantly improving the coarsening resistance of the $L1_2$-precipitates (by a factor four), and the thermal stability of the α-precipitates [7, 27, 28]. Herein, we report on the effects of a further addition of

W, which is an extremely slow diffuser in Al similar to Mo, $D_W = 5 \times 10^{-23}$ m^2s^{-1}, compared to $D_{Mo} = 6 \times 10^{-23}$ m^2s^{-1} at 400 °C [26]. We added W to an Al-Mn-Mo-Si-Zr-Sc-Er alloy, focusing on the change of kinetics of $L1_2$- and α-precipitates, the coarsening resistance, and creep resistance of the alloy.

An Al-0.26Mn-0.11Mo-0.11Si-0.08Zr-0.02Sc-0.01Er-0.025W (at.%) alloy was prepared by melting 99.99 % pure Al and Al-X (X = Mn, Mo, Si, Zr, Sc, Er, W) master alloys, and casting the melt in a graphite cylindrical mold (37 mm diameter): Ref. [23] for more details. Table 1 provides the composition of the new W-modified alloy (W solubility limit at 640 ºC is ~ 0.025 at.% [29]) and its W-free counterpart, whose composition was reported in Ref. [24]. Both alloys have an optimal homogenization time of 2 h at 640 °C, which results in the highest microhardness after the alloy is peak-aged at 400 °C for 24 h. Homogenization of the alloys at 640 °C would dissolve the Er-rich primary precipitates (a beneficial effect, as it results in more Er in solid-solution for later nano-precipitation on aging). The process, however, also cause the precipitation of coarse $Al_3(Zr,Sc)$ phases, which is detrimental because it depletes Zr and Sc from the matrix, making them unavailable for nano-precipitation on subsequent aging. The chosen 2 h homogenization time is a compromise between these two effects. During processing, we used a fast heating rate (preheated furnace) to reduce the formation of coarse $Al_3(Zr,Sc)$ precipitates.

Table 1. Compositions in at.% (values in wt.% in parentheses) of the two W-free and W-modified Al-alloys, measured by inductivity-coupled argon plasma atomic-emission spectrometry (ICAP-AES) at Genitest Inc (Montréal, QC).

Alloys	Mn	Mo	Si	Zr	Sc	Er	W	Fe

W-modified alloy	0.258 (0.520)	0.114 (0.400)	0.107 (0.110)	0.081 (0.270)	0.018 (0.030)	0.005 (0.032)	0.025 (0.170)	0.005 (0.010)
W-free alloy [24]	0.250 (0.505)	0.108 (0.381)	0.107 (0.111)	0.080 (0.268)	0.024 (0.397)	0.009 (0.055)	-	<0.005 (<0.010)

To study the precipitation kinetics of the homogenized W-modified alloy, isochronal aging was performed from 100 to 575 °C, with steps of 25 °C for 3 h (effective warming rate ~ 8.3 °C/h). Each step was terminated by water quenching. Figure 1a displays the evolution of the Vickers microhardnesses of the W-modified and W-free alloys as a function of aging temperature, measured on polished samples (1 μm surface finish, sample dimension ~ 1 cm × 1 cm × 3 mm) using a Struers Duramin-5 microhardness tester, with a load of 200 gf and a dwell time of 5 s. While the two curves generally have the same shape and the same peak microhardness of ~ 620 MPa, the W-modified alloy reaches its peak microhardness at 400 °C vs. 450 °C for the unmodified alloy; at 475 °C, the W-free alloy maintains the peak microhardness (within error), while the W-modified alloy's microhardness has significantly decreased, by ~ 63 MPa from its peak value. In cast Al alloys, with the low dislocation density and large grain sizes, the primary contributing factor to the resistivity is the solute content in the matrix. During different stages of isochronal aging, precipitates may nucleate, grow, coarsen, or dissolve, changing the solute content in the matrix, thus altering the electrical resistivity. Therefore, the change of electrical conductivity would provide information on the precipitation process. Figure 1b (top half) demonstrates that the W micro-addition significantly alters the evolution of the electrical conductivity (measured using a Sigmatest 2.069 eddy current instrument on samples of dimension ~ 1 cm × 1 cm × 3 mm). To illustrate this more clearly, the normalized negative derivative of the resistivity

as a function of temperature is presented in the bottom half of Figure 1b, highlighting the temperatures at which the resistivity changes significantly due to precipitation [30]. For both alloys, two peaks are identified, associated with Al_3Zr (as outer shells of the $L1_2$-precipitates) and α-Al(Mn,Mo)Si precipitates, respectively. The peaks associated with precipitation of Al_3Er and Al_3Sc (as cores of the $L1_2$-precipitates) cannot be identified clearly due to the small concentrations of Er and Sc. It is evident from Figure 1b, with a W micro-addition, that the peak associated with $L1_2$-precipitation is shifted to a lower temperature (from 375 °C, shown as a shoulder of the larger peak associated with α-Al(Mn,Mo)Si precipitation, to 350 °C), while the peak associated with α-precipitation is shifted to a higher temperature (from 450 to 500 °C). Figure 1c displays a scanning electron microscopy (SEM) back-scattered electron (BSE) micrograph of the W-modified alloy over-aged isochronally to 475 °C. For this and other samples aged isochronally to >475 °C, α-precipitates are observed using SEM (characterized by their elongated shape), consistent with the electrical conductivity (EC) evolutionary trend.

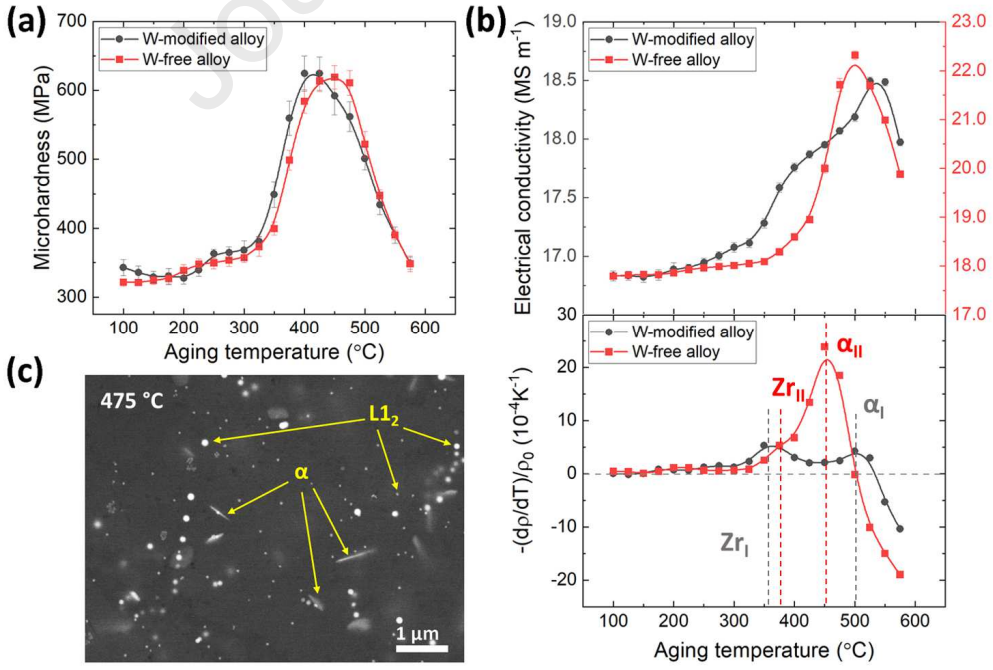

Figure 1. Evolution of: (a) microhardness; (b) electrical conductivity (EC) and corresponding negative temperature derivatives of the resistivity (normalized by the initial resistivity) of the W-free [24] and W-modified alloys, during isochronal aging from 100 °C to 575 °C (3 h steps). Peaks related to different precipitation processes are indicated by vertical dashed lines (red and black); and (c) SEM back-scattered electron micrograph showing the precipitate microstructures after isochronally aging the W-modified alloy to 475 °C. Micron-sized α-Al(Mn,Mo)Si precipitates (created during aging) and sub-micron $L1_2$-Al_3(Zr,Sc) precipitates (created during homogenization) are visible at this magnification, but not the nanosized $L1_2$-Al_3(Zr,Sc) formed on aging.

The isochronal aging results (Figure 1) indicate that tungsten at a micro-addition level of 0.025 at.% (0.17 wt.%) alters significantly the precipitation kinetics of both the $L1_2$- and α-precipitates. We now discuss how interactions of W atoms with the $L1_2$- and α-forming elements, and/or with vacancies in the Al matrix, may be affecting the precipitation kinetics, either directly or indirectly. Figure 1 demonstrates that a W addition affects mainly the $L1_2$-precipitates in the growth regime when $L1_2$-precipitates grow by imbibing Zr atoms, rather than in the subsequent coarsening regime, because the shift of the Zr precipitation peak occurs at the range of temperatures (around 350 ºC), where the electrical conductivity increases continuously, which is a characteristic of the growth regime. Considering the small concentration and the sluggish diffusion of W in Al as well as the strong repulsive W-Al vacancy interaction [31], it is unlikely that W assists Zr diffusion in the Al-matrix by forming stable Zr-W-vacancy trimers and decreasing the Zr migration energy, a mechanism akin to that of Si assisting Sc diffusion and precipitation in an Al-matrix [32]. This is because this mechanism would require long-

range diffusion of Zr-W-vacancy trimers between nanoprecipitates separated by tens of nanometers (~23 nm for the peak-aged condition, according to APT data), which is not credible given a typical diffusion distance of $x = (6Dt)^{1/2} < 2$ nm for W in Al (at 400 ºC for t = 3 h) [33]. Therefore, the effects of W are more likely to be localized in the vicinity of $L1_2$-precipitates, where W may be enriched.

To investigate this hypothesis, atom-probe tomography (APT) analyses were performed on the W-modified alloy aged isothermally at 400 °C for 1, 11, and 21 days, corresponding to a peak-aged condition (1 day) and two over-aged conditions (11 and 21 days), respectively. Standard electropolishing technique [7] was used to prepare APT tips with tip radius ~ 50 nm. Figure 2 displays the proximity histograms, revealing the solute concentrations across the matrix/$L1_2$ interface (marked with a dashed line). The concentration profiles exhibit a typical core-shell structure, with Er, Si, Sc and Mn enriched in the core, and Zr, Mo, and W enriched in the shell. Molybdenum has the highest concentration near the Al-matrix(f.c.c.)/$L1_2$ heterophase interface, but a significant amount of Mo also partitions to the precipitate core. Comparing with APT investigations performed on the W-free alloy [7], the partitioning behaviors of Er, Sc, Zr, Si, Mn, and Mo within the $L1_2$-precipitates are not affected significantly by W microalloying. Tungsten enrichment at the Al-matrix(f.c.c.)/$L1_2$ heterophase interface implies that W is reducing the interfacial free energy and perhaps strain energy to a certain degree around the $L1_2$- precipitates, given that W is not a $L1_2$-forming element (such as Er, Sc and Zr).

As indicated by the isochronal aging results, the accelerated Al_3Zr precipitation kinetics in the W-modified alloy occurs at temperatures ranging from 300 to 350 °C. At these

temperatures, the equilibrium vacancy concentration can be estimated using a vacancy formation enthalpy of 0.75 eV and formation entropy of 0.23*k* in pure Al (*k* is Boltzmann's constant) [34]. At the temperatures of interest (300 – 350 °C), the number density of the vacancies is on the order of 10^{23} m^{-3}: Supplementary Information, SI. This number density is of the same order of magnitude as the $L1_2$ precipitate number density at the early stage of precipitation; for example, the peak-aged condition for a 400 °C isothermal aging treatment the number density is 7.9×10^{22} m^{-3}. Even though the Al-matrix(f.c.c.)/$L1_2$ heterophase interface is coherent and unlikely to be good sinks for vacancies. The vacancies can, however, be trapped at chemical interfaces in this phase separated alloy, decreasing the concentration of freely migrating vacancies [35]. The implication from the comparable number density of vacancies and $L1_2$-precipitates is that, at 300 – 350 °C, only a few vacancies are responsible for the growth of each precipitate. Because the vacancies spend time diffusing around the Al-matrix(f.c.c.)/$L1_2$ heterophase interfaces (chemically trapped), there are fewer freely migrating vacancies available to transport solute atoms from matrix to the precipitate until the vacancies are emitted back into the matrix. Modification of the interface chemistry by W local enrichment, plus the repulsive W-vacancy interaction [31], may lead to less trapping and alter the precipitation kinetics. Note that in the cast Al alloys, the dislocation density is low, ~ $10^{12}/m^2$ [36], thus a subtle change in the precipitate/vacancy interaction would have a meaningful effect on the overall vacancy concentration in the matrix. The suggested mechanism is consistent with the isochronal aging observation that, in the W-modified alloy, Zr commences to precipitate at a temperature lower by 25 °C than in the W-free alloy.

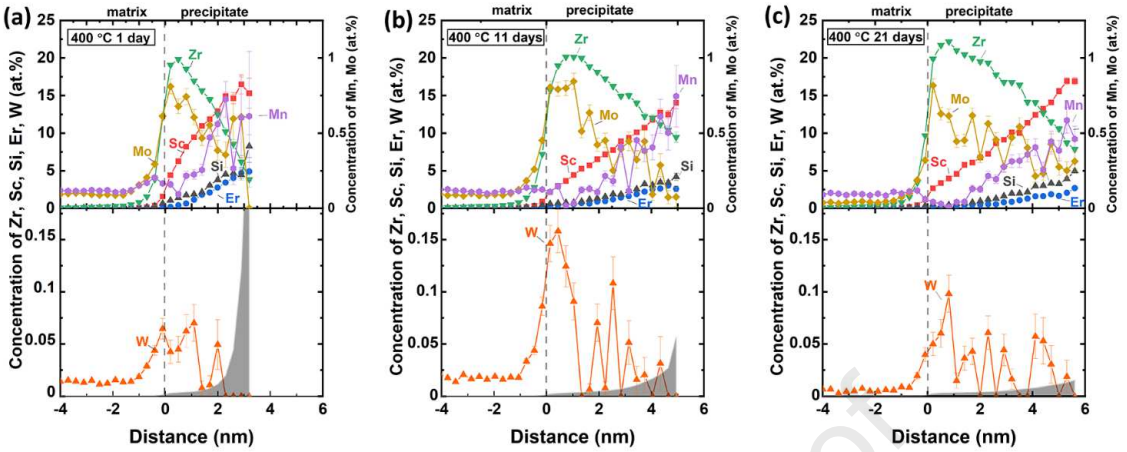

Figure 2. Concentration profiles obtained from proximity histograms of the $L1_2$-$Al_3(Zr,Sc)$ nanoprecipitates observed in the W-modified alloy homogenized for 2 h, and then aged at 400 °C for: (a) 1 day; (b) 11 days; and (c) 21 days. Elemental partitioning occurs in the precipitate, resulting in a core-shell structure. The grey areas visible in (a) and (b) represent the detection limit, that is, the concentration for which the bin contains only one solute atom.

Unlike the $L1_2$-precipitates, the α-Al(Mn,Mo)Si precipitates exhibit, in the W-modified alloy, a delayed precipitation during isochronal aging. We have demonstrated previously, using APT, that in an arc-melted W-modified Al-Mn-Mo-Si-Zr-Sc-Er alloy with a similar composition (the same 0.025 at.% W addition), similarly aged isothermally at 400 °C, that W partitions to the α-precipitates at ~ 0.1 at.% level [37]. Whether such partitioning alters significantly the thermal stability of the α-precipitates and the driving force for precipitation is, however, unclear. The previously discussed vacancy trapping effect at the Al-matrix(f.c.c.)/$L1_2$ heterophase interfaces is not important in the temperature range 450 – 500 °C, because at these temperatures, the thermal equilibrium vacancy number density is at least two order of magnitude greater than number density of $L1_2$-precipitates.

Another possible mechanism relies on W-solute interactions. Farkoosh et al. [38] calculated W-Si interactions using first-principles calculations, and calculated that W and Si exhibit a small attractive interaction energy of ~ 0.041 eV/atom at 0 K. Given the sluggish diffusivity of W and the repulsive interaction energies between W and an Al-vacancy dimer, Si atoms could be trapped by W atoms, due to thermodynamic (an attractive W-Si binding free energy) and kinetic (smaller local vacancy concentration near W atoms, due to a repulsive free binding energy, compared to that of a random vacancy distribution). Therefore, the α-Al(Mn,Mo)Si precipitation process could be retarded due to both the limited availability of Si atoms and the reduced mobility of Si atoms in the Al-matrix (f.c.c.). This mechanism for delaying the coarsening of α-precipitates does not require long-range diffusion of W atoms.

The APT results, together with the Vickers microhardness evolution (Figure 3), also provide insights on the effects of W micro-additions on the coarsening resistance of the alloy. Table 2 lists the precipitate number density, mean radius, and volume fraction of both the W-modified and W-free alloys after various heat-treatments. Upon isothermal aging at 400 °C, the W-modified alloy exhibits a higher precipitate number density and slightly smaller precipitate radii (the difference is within one standard deviation) compared to the W-free alloy with the same heat-treatment. Due to the small APT nanotip volume and the non-uniform spatial distribution of the $L1_2$- precipitates within and in between the dendrites, the APT results are supplemented with TEM observations: see SI. The precipitate radii measured by both techniques are consistent with one another. At the early stage of isothermal aging (aging time < 1 h), the microhardness of the two alloys are almost identical, Figure 3. For an aging time longer than 1 h, the microhardness

of the W-modified alloy starts to deviate from that of the W-free alloy, reaching a peak-microhardness (at 1 day) of ~ 634 MPa, higher than the peak-microhardness of the W-free alloy (604 MPa). The higher peak-microhardness of the W-modified alloy is consistent with the higher $L1_2$-precipitate number density and smaller precipitate radii, as measured by APT. When over-aged the microhardness of the W-modified alloy appears to decrease, however, at a slightly higher rate, eventually reaching the same value of the W-free alloy at an aging time of 3 months.

Table 2. Precipitate number density, mean radius, and volume fraction of both the W-modified and W-free alloys after various heat-treatments.

Alloy	Aging treatment at 400 ºC in days	N_V ($\times 10^{22}$ m^{-3})	$\langle R(t) \rangle$ (nm)	φ (%)
W-modified Alloy	400 ºC / 1	7.9 ± 0.5	2.6 ± 0.5	0.48 ± 0.03
	400 ºC / 11	2.4 ± 0.2	3.2 ± 0.8	0.42 ± 0.04
	400 ºC / 21	0.9 ± 0.1	3.8 ± 0.9	0.28 ± 0.04
W-free Alloy [7]	400 ºC / 1	2.7 ± 0.4	2.9 ± 0.6	0.34 ± 0.05
	400 ºC / 11	0.9 ± 0.2	3.9 ± 1.5	0.40 ± 0.07

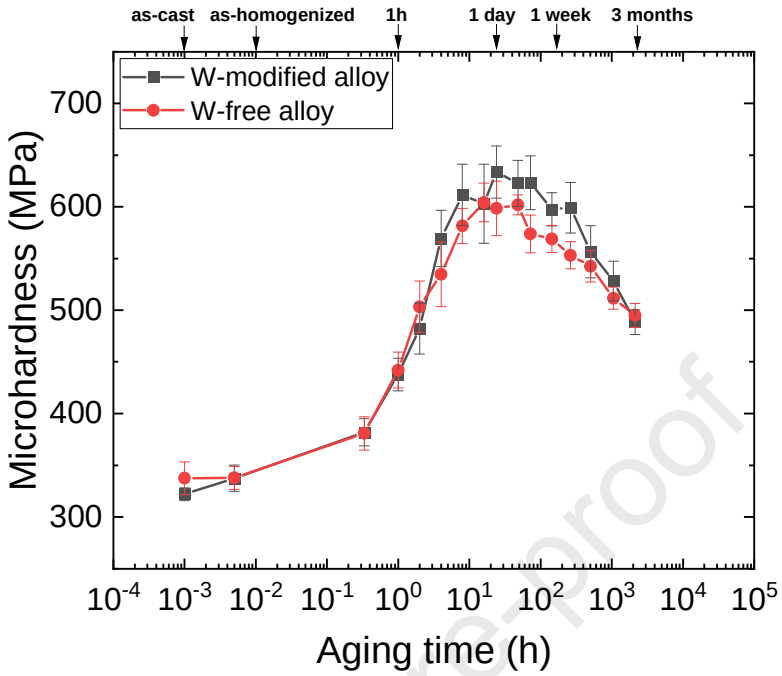

Figure 3. Evolution of Vickers microhardness of the W-modified alloy and the W-free alloy at 400 °C as a function of aging time. Data for the W-free alloy is from Ref. [24]. The heat-treatment procedure in Ref. [24] is the same as in this work.

Compressive creep experiments were performed at 300 °C on samples aged isothermally at 400 °C for 1 day (peak-aging) and for 11 and 21 days (over-aging). Figure 4 displays the creep behavior of the W-modified alloy and the W-free alloy [24]. As summarized in Table 3, creep threshold stress values, σ_{th}, were determined by fitting creep data to a modified power-law (details on fitting in SI and Ref. [7]).

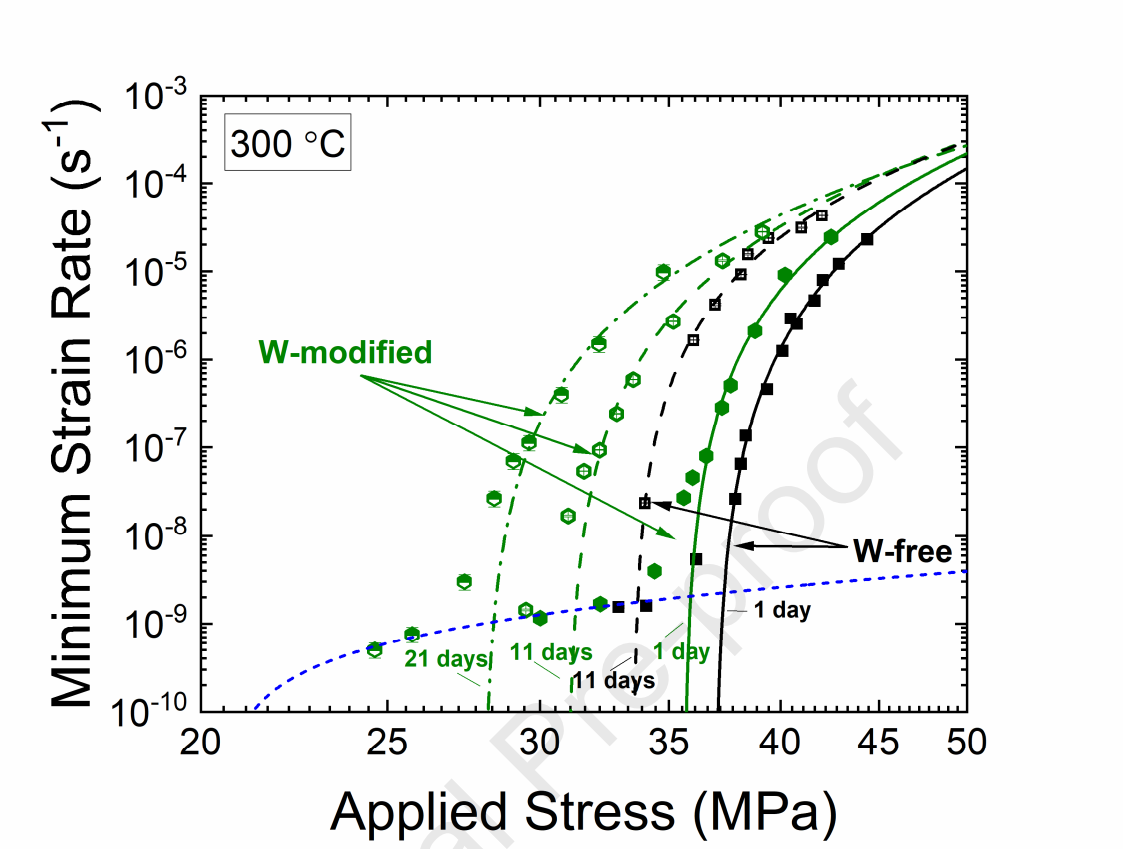

Figure 4. Double-logarithmic plot of minimum compressive creep strain rate (300 °C) as a function of applied compressive stress for both the W-modified (different green symbols) and W-free (open- and solid-black symbols) alloys [7]. Employing the multi-variable non-linear regression analysis, the dislocation creep portion of the curves is fitted using n = 3 (black and green curves) and the diffusional creep using n=1 (blue). Prior to the creep experiments, the samples were aged isothermally at 400 °C for 1 day (filled symbols, solid lines), 11 days (open symbols, dashed lines) and 21 days (half-filled symbols, green dash-dot lines).

Table 3. Threshold stresses for compressive creep at 300 °C for both W-modified and W-free alloys after various pre-creep heat treatments.

Alloy	Pre-creep heat treatment	Pre-creep, aged microhardness (MPa)	Threshold stress σ_{th} for creep at 300 °C (MPa)
W-modified alloy	400 ºC / 1 day	634 ± 25	35.6 ± 0.1
	400 ºC / 11 days	599 ± 24	31.0 ± 0.1
	400 ºC / 21 days	556 ± 25	28.0 ± 0.3
W-free alloy [7]	400 ºC / 1 day	602 ± 9	37.0 ± 0.1
	400 ºC / 11 days	542 ± 15	33.9 ± 0.1

Several observations are evident from Figure 4 and Table 3. First, for both alloys, the peak-aged sample (400 ºC for 1 day) exhibits the highest creep resistance, while the over-aged samples exhibit a decreased creep resistance. This is consistent with prior experiments of Mn/Si-bearing $L1_2$-strengthened alloys, and can be explained by a reduced Mn/Si solid-solution strengthening mechanism as α-precipitates undergo coarsening, which more than counterbalances the slight coarsening of $L1_2$-precipitates (anticipated to improve creep resistance due to increased coherency strains around precipitates) [7]. Additionally, for the same pre-creep heat-treatment, the W-modified alloy exhibits a slightly smaller threshold stress compared to the W-free alloy, which manifests itself as a shift of the curves by a few MPa toward lower values. Micro-additions of W affect the precipitate volume-fraction, mean precipitate radii and number density (Table 2), and ultimately edge-to-edge inter-precipitate distances, which all affect the creep resistance of alloys. As the volume fraction of $L1_2$-nanoprecipitates appears higher in the W-modified alloy, it is expected that the alloy would exhibit improved creep resistance, which, however, is not the case. A likely explanation would be that the presence of W in the $L1_2$-nanoprecipitates affects negatively the overall

matrix/precipitate lattice-parameter mismatch. Employing the APT experiments, we are able to measure the nanoprecipitates composition, Table 4, and calculated lattice parameters assuming Vegard's rule, using the lattice parameters of $L1_2$-Al_3Er (4.232 Å), -Al_3Sc (4.125 Å) and -Al_3Zr (4.105 Å). Using this approach, we are not able, however, to find evidence for a significant difference between the W-free and W-containing alloys. Accurate estimations of W-induced lattice parameter changes would require casting bulk $L1_2$-Al_3M alloys, which is beyond the scope of this project, but would provide useful knowledge. Given these uncertainties, we cannot attribute the small difference in the threshold stress (~ 2 MPa, a relative change of <8%) between the W-modified and W-free alloys to a particular mechanism, but we nevertheless conclude that W micro-additions do not alter significantly the dislocation creep resistance of the Al-Mn-Mo-Si-Zr-Sc-Er alloy, at least at the investigated concentrations. It is noteworthy mentioning that at low strain rates ($<2\times10^{-9}$ s^{-1}), all three creep curves of the W-modified alloy deviate significantly from the fit of a dislocation creep model, which suggests that diffusional creep is active. As all the data points appear to fall in line, it indicates that the pre-heat treatment does not influence significantly the diffusional creep rate. Employing Eq.S1 (see SI) and n = 1, a good fit can be obtained for all the low-strain-rate data points, estimating a diffusional creep threshold stress of 20.5 ± 0.8 MPa. It is interesting that the low strain rate data points of the W-free alloy fall onto the diffusional creep fit line, indicating that W does not induce any particular change (positive or negative) to the diffusion creep resistance in the W-containing alloy.

Table 4. Average precipitate compositions of the W-modified alloy measured by atom-probe tomography, with the lattice parameter mismatches calculated using the compositional data.

Alloy	Aging time at 400 ºC (days)	Precipitate composition (at.%)								$L1_2$/matrix lattice mismatch at 300 °C (%)
		Al	Er	Sc	Zr	Si	Mn	Mo	W	
W-modified Alloy	1	71.55	0.98	7.62	17.07	1.81	0.24	0.67	0.05	1.67
	11	72.88	0.95	6.25	17.71	1.41	0.17	0.56	0.06	1.65
	21	73.22	0.52	5.93	18.71	0.88	0.16	0.54	0.05	1.59
W-free Alloy [7]	1	72.3	0.4	6.2	18.9	1.3	0.2	0.8	-	1.65
	11	72.2	1.3	8.9	14.5	2.2	0.4	0.5	-	1.63

In summary, we examined the effects of a W micro-addition on the precipitation kinetics and coarsening resistance of an Al-Er-Sc-Zr-Mn-Mo alloy. Isochronal aging results indicate that W accelerates the precipitation of $L1_2$-Al_3(Zr,Sc)-precipitates, but retards the precipitation of α-Al(Mn,Mo)Si-precipitates. The former effect may be attributed to the observed local enrichment of W atoms at the Al-matrix(f.c.c.)/$L1_2$ heterophase interfaces, which is hypothesized to reduce vacancy trapping at the interface and thus increase the matrix vacancy concentration and concomitantly Zr diffusion in the matrix. The latter effect is consistent with an attractive W-Si interaction, which reduces Si's availability and mobility and concomitantly the precipitation kinetics of α-Al(Mn,Mo)Si precipitates. Tungsten micro-additions increase the peak-microhardness of the alloy during isothermal aging but does not improve the coarsening resistance and creep resistance.

Acknowledgments - This research was sponsored by the Ford-Northwestern University Alliance. The authors thank Drs. J.M. Boileau and B. Ghaffari (Ford Motor Company) for numerous useful discussions. DNS and DCD also acknowledge partial support (for the redaction of the manuscript) from the Office of Naval Research, under grant N00014-16-1-2402. Atom-probe tomography was performed at the Northwestern University Center for Atom-Probe Tomography (NUCAPT). The LEAP tomograph in NUCAPT was purchased and upgraded with funding from NSF-MRI (DMR-0420532) and ONR DURIP (N00014e0400798, N00014e0610539, N00014-0910781, N00014-1712870) programs. Instrumentation at NUCAPT was partially supported by the Initiative for Sustainability and Energy at Northwestern University (ISEN). This work made use of the MatCI Facility and the EPIC facility (NUANCE Center) at Northwestern University. NUCAPT, MatCI and NUANCE received support from the MRSEC program (NSF DMR-1720139) through Northwestern's Materials Research Center; NUCAPT and NUANCE also benefitted from the Soft and Hybrid Nanotechnology Experimental (SHyNE) Resource (NSF NNCI-1542205). NUANCE received support from the International Institute for Nanotechnology (IIN); the Keck Foundation; and the State of Illinois, through the IIN. DNS and DCD disclose financial interests in NanoAl LLC and Braidy Industries LLC, which are active in the area of aluminum alloys.

Data Availability

The raw/processed data required to reproduce these findings cannot be shared at this time as the data also forms part of an ongoing study.

References

[1] M.E. Drits, J. Dutkiewicz, L.S. Toropova, J. Salawa, Crystal Research and Technology 19(10) (1984) 1325-1330.
[2] E.A. Marquis, D.N. Seidman, Acta Mater. 49(11) (2001) 1909-1919.
[3] C. Watanabe, T. Kondo, R. Monzen, Metall and Mat Trans A 35(9) (2004) 3003-3008.
[4] W. Kang, H.Y. Li, S.X. Zhao, Y. Han, C.L. Yang, G. Ma, Journal of Alloys and Compounds 704 (2017) 683-692.
[5] T. Dorin, M. Ramajayam, S. Babaniaris, T.J. Langan, Materials Characterization 154 (2019) 353-362.
[6] Q. Dong, A. Howells, M.F. Gallerneault, V. Fallah, Acta Mater. 186 (2020) 308-323.
[7] S. Shu, A. De Luca, D.C. Dunand, D.N. Seidman, Materials Science and Engineering: A 800 (2021) 140288.
[8] R.A. Karnesky, M.E. van Dalen, D.C. Dunand, D.N. Seidman, Scr. Mater. 55(5) (2006) 437-440.
[9] R.A. Karnesky, D.N. Seidman, D.C. Dunand, Materials Science Forum 519-521 (2006) 1035-1040.
[10] Y. Zhang, J. Gu, Y. Tian, H. Gao, J. Wang, B. Sun, Materials Science and Engineering: A 616 (2014) 132-140.
[11] R.Y. Barkov, A.V. Pozdniakov, E. Tkachuk, V.S. Zolotorevskiy, Mater. Lett. 217 (2018) 135-138.
[12] C.B. Fuller, D.N. Seidman, D.C. Dunand, Acta Mater. 51(16) (2003) 4803-4814.
[13] M.E. van Dalen, D.C. Dunand, D.N. Seidman, Acta Mater. 53(15) (2005) 4225-4235.
[14] J. Taendl, A. Orthacker, H. Amenitsch, G. Kothleitner, C. Poletti, Acta Mater. 117 (2016) 43-50.
[15] D. Erdeniz, W. Nasim, J. Malik, A.R. Yost, S. Park, A. De Luca, N.Q. Vo, I. Karaman, B. Mansoor, D.N. Seidman, D.C. Dunand, Acta Mater. 124 (2017) 501-512.
[16] Y. Fan, M.M. Makhlouf, Journal of Alloys and Compounds 725 (2017) 171-180.
[17] P. Yu, M. Yan, D. Tomus, C.A. Brice, C.J. Bettles, B. Muddle, M. Qian, Materials Characterization 143 (2018) 43-49.
[18] N.Q. Vo, D.C. Dunand, D.N. Seidman, Acta Mater. 63 (2014) 73-85.
[19] J.D. Lin, P. Okle, D.C. Dunand, D.N. Seidman, Materials Science and Engineering: A 680 (2017) 64-74.
[20] P. Okle, J.D. Lin, T. Zhu, D.C. Dunand, D.N. Seidman, Materials Science and Engineering: A 739 (2019) 427-436.
[21] A. De Luca, D.C. Dunand, D.N. Seidman, Acta Mater. 119 (2016) 35-42.
[22] K.E. Knipling, D.C. Dunand, D.N. Seidman, Acta Mater. 56(1) (2008) 114-127.
[23] A. De Luca, D.C. Dunand, D.N. Seidman, Acta Mater. 144 (2018) 80-91.
[24] A. De Luca, S. Shu, D.N. Seidman, Materials Characterization 169 (2020) 110585.
[25] A. De Luca, D.N. Seidman, D.C. Dunand, Acta Mater. 165 (2019) 1-14.
[26] K.E. Knipling, D.C. Dunand, D.N. Seidman, Zeitschrift für Metallkunde 97(3) (2006) 246-265.

[27] A.R. Farkoosh, X. Grant Chen, M. Pekguleryuz, Materials Science and Engineering: A 620 (2015) 181-189.
[28] S. Shu, A. De Luca, D.N. Seidman, D.C. Dunand, Effects of Mn and Mo Micro-additions on Al–Zr–Sc–Er–Si Mechanical Properties, in: A. Tomsett (Ed.) Light Metals 2020, Springer International Publishing, Cham, 2020, pp. 312-317.
[29] V.N. Vigdorovich, V.M. Glazov, N.N. Glagoleva, Izv. Vyssh. Uch. Zaved., Istvet. Met. (2) (1960) 143-146.
[30] M. Vlach, I. Stulíková, B. Smola, N. Žaludová, J. Černá, Journal of Alloys and Compounds 492(1) (2010) 143-148.
[31] D. Simonovic, M.H.F. Sluiter, Phys. Rev. B 79(5) (2009) 054304.
[32] C. Booth-Morrison, Z. Mao, M. Diaz, D.C. Dunand, C. Wolverton, D.N. Seidman, Acta Mater. 60(12) (2012) 4740-4752.
[33] N. van Chi, D. Bergner, in: F.J. Kedves, D.L. Beke (Eds.), DIMETA-82: Diffusion in Metals and Alloys, Trans Tech Publications, Switzerland, 1983, p. 334.
[34] T. Hehenkamp, Journal of Physics and Chemistry of Solids 55(10) (1994) 907-915.
[35] S. Shu, P. Bellon, R.S. Averback, Phys. Rev. B 91(21) (2015) 214107.
[36] V.S. Zolotorevsky, N.A. Belov, M.V. Glazoff, in: V.S. Zolotorevsky, N.A. Belov, M.V. Glazoff (Eds.), Casting Aluminum Alloys, Elsevier, Amsterdam, 2007, pp. 95-182.
[37] A. De Luca, D.N. Seidman, D.C. Dunand, Dual precipitation-strengthening in Al-Mn-Zr-Sc-based alloys microalloyed with refractory elements, (Unpublished results).
[38] A.R. Farkoosh, D.C. Dunand, D.N. Seidman, Effect of W and Si Microadditions on Microstructure and Strength of Dilute, Precipitation-Strengthened Al-Zr-Er Alloys, (unpublished).

Originality Statement

I write on behalf of myself and all co-authors to confirm that the results reported in the manuscript are original and neither the entire work, nor any of its parts have been previously published. The authors confirm that the article has not been submitted to peer review, nor has been accepted for publishing in another journal. The author(s) confirms that the research in their work is original, and that all the data given in the article are real and authentic. If necessary, the article can be recalled, and errors corrected.

Declaration of interests

☐ The authors declare that they have no known competing financial interests or personal relationships that could have appeared to influence the work reported in this paper.

☒The authors declare the following financial interests/personal relationships which may be considered as potential competing interests:

David N. Siedman and David C. Dunand disclose financial interests in NanoAl LLC and Braidy Industries, which are active in the area of aluminum alloys.